

Superconductivity in nanocrystalline tungsten thin films growth by sputtering in a nitrogen-argon mixture

J. A. Hofer,^{1*} N. Haberkorn^{1,2}

¹ Comisión Nacional de Energía Atómica and Consejo Nacional de Investigaciones Científicas y Técnicas, Centro Atómico Bariloche, Av. Bustillo 9500, 8400 San Carlos de Bariloche, Argentina.

² Instituto Balseiro, Universidad Nacional de Cuyo and Comisión Nacional de Energía Atómica, Av. Bustillo 9500, 8400 San Carlos de Bariloche, Argentina.

We report on the structural and superconducting properties of nanocrystalline tungsten thin films growth by sputtering at room temperature with an N₂:Ar mixture (N₂ from 3% to 50%). The crystalline phases were identified by comparing pristine and thermal annealed thin films. For N₂/(Ar+N₂) mixtures between 3 and 10 %, the films display nanocrystalline β-W phase. Coexistence of β-W and W₂N phases are observed for gas mixtures with N₂ between 20 % and 40%. A detailed study of the superconducting properties as function of the thickness was performed for W films growth with 8 % N₂ mixtures. For this concentration, the nitrogen atoms increase the disorder at the nanoscale reducing the grain size and avoiding the crystallization of α-W. The superconducting critical temperature ($T_c = 4.7$ K) is thickness independent for films thicker than ~ 17 nm. Below this thickness, the T_c value decreases systematically being 3.1 K for 4 nm thick films. Our study provides a simple method for the fabrication of nanocrystalline β-W thin films with potential applications in superconducting devices.

Keywords: sputtering; tungsten; superconductivity.

Email: juan.hofer@cab.cnea.gov.ar

1. Introduction

Tungsten is a metal with several applications in micro-electromechanical devices [1,2]. W films exist in two allotropic forms: alpha (α)-W (body-centered cubic structure) and beta (β)-W (A15 structure). The electrical resistivity of α-W is always lower than the electrical resistivity of β-W. A distinctive feature of W is that displays superconductivity [3,4]. The superconducting critical temperature T_c can be enhanced from 12 mK for α-W to up 5.2 K for the coexistence of β-W and amorphous structures [1,2,5,6]. The

properties and structure of W thin films depend on the growth conditions [7,8]. The synthesis of amorphous-like tungsten has been reported in thin films growth with an Ar/O₂ atmosphere [9]. In addition, superconductivity with $T_c \approx 4.85$ K has been reported for thin films growth in a reactive Ar/N₂ atmosphere close to the phase boundary between β -W and W₂N [10]. The comparison between thin films growth in Ar/O₂ and Ar/N₂ atmosphere suggests that, for certain gas mixtures, the oxygen and nitrogen impurities stabilize amorphous phases.

In this work, we analyze the presence of superconductivity in nanometric grain size W thin films growth at room temperature in an N₂/Ar mixture (N₂ from 3% to 50%). The results show that the microstructure, crystalline structure and the presence of superconductivity depend on the N₂ concentration in the gas mixture. The comparison between pristine and thermal annealed films shows that the superconductivity can be related to nanocrystalline β -W phase and amorphous phases. We study in detail the superconducting properties for films growth with an 8% N₂ mixture. For this concentration, no features related with W₂N were observed for X-ray diffraction in pristine and thermal annealed films (nitrogen is mainly an interstitial impurity). The study of the superconducting properties was performed for films with thickness between 3 nm and 160 nm. The superconducting critical temperature ($T_c = 4.7$ K) is thickness independent for films thicker than ~ 17 nm. Below this thickness, the T_c value decreases systematically being 3.1 K for 4 nm thick films. The analysis of the upper critical fields indicates that the extrapolated value at zero increases as the films thickness decreases, which can be related to changes in the microstructure and reduction in the grain size average.

2. Materials and methods

W films were deposited on Si (100) wafers by sputtering in an Ar / N₂ mixture. The substrates (≈ 1 cm²) were etched with HF 6%. The films were grown using a power of 50 watts with a 99.99% purity W target (diameter: 38 mm). The substrate temperature was modified from room temperature (RT) to 673 K. The base pressure was $\approx 5 \times 10^{-7}$ Torr. The total pressure during the deposition of the films was kept constant in 5 mTorr. The N₂ partial pressure was modified from 3% to 50%. Ultra-high purity Ar (99.999%) and N₂ (99.999%) were used as gas sources. Thermal annealing was performed in a vacuum atmosphere ($\approx 1 \times 10^{-6}$ Torr) at 973 K. Wherever used, the notation [dWX-T],

indicates a tungsten film with a thickness of d [nm], and X nitrogen [%] mixture and T the growth temperature [K], respectively.

X-ray diffraction (XRD) was used to characterize the crystal structure of the films (Panalytical Empyrean equipment). The film thickness was calibrated by low-angle X-ray reflectivity (XRR). Profile fitting was done using the Parratt32 code [11]. The electrical transport measurements were performed on 1 mm (length) x 0.02 mm (width) bridges using the standard four-terminal transport technique.

3. Results and discussion

3.1. Influence of the N_2/Ar mixture on the crystalline structure and electrical transport of W thin films

Figure 1 shows the XRD pattern for W films growth using different $N_2:Ar$ mixtures. The results show that for N_2 mixtures up to 10 %, the XRD patterns display the (200) and (210) reflections of the β phase. For N_2 mixtures between 20% and 40%, the XRD patterns display a wide reflection at $2\theta \sim 38.5^\circ$. The peak is shifted to $2\theta \sim 36.45^\circ$ in [138W50-RT], which could be related with microstructural and stoichiometric changes. The grain size average (D), extracted from the analysis of the peak width using the Scherrer formula, decreases as the N_2 in the mixture (the exception is [138W50-RT]). The estimated D values are 9 nm for [160W8-RT], 6.7 nm for [160W10-RT], 2.1 nm for [155W20-RT], 1.8 nm for [145W30-RT] and 7.9 nm for [138W50-RT]. It is important to note that sputtering usually produces columnar structures, which implies that the grains could be elongated at the growth direction. To analyze in detail the origin of the peaks in the XRD patterns, the films were annealed at 973 K for 1 hour in vacuum. Figure 1b shows the results for [160W8-RT], [155W20-RT], [145W30-RT] and [138W50-RT]. Thin films growth with N_2 concentration up to 10% display phase coexistence between α -W and W_2N (minority phase), which suggests that the nitrogen in the films growth at RT is an interstitial impurity. The D value for α -W is ≈ 17 nm. Thin films with mixtures between 20 % and 30 % display coexistence of W_2N ($D \approx 40$ nm and 70 nm, respectively) and metallic W (minority phase). The shift to lower angles of the reflection in [138W50-RT] suggests a different N stoichiometry. However, the reflection in $2\theta \approx 37.0^\circ$ does not agree neither with WN nor $W_{0.75}N$. The D value is ≈ 12 nm.

Figure 2 shows a summary of the electrical transport for thin films growth using different N_2 mixtures. Most of the films display superconductivity with T_c between 3 K

and 4.9 K (see Fig. 2a). The exception is [155W20-RT]. The T_c values are in the range of amorphous W [5,6]. Moreover, for N_2 mixtures lower than 10%, the fluctuations in T_c are similar to that reported in ref. [8]. We attribute the presence of superconductivity for N_2 mixtures richer than 20% to the coexistence of amorphous W and nitrides. The disorder at the nanoscale for all the films is evident from the low value of the residual resistivity ratio ($RRR = R^{300K}/R^{10K} \approx 0.9-0.97$ (not shown)). Following the analysis of the structural and superconducting properties will be focused on thin films growth using an 8 % N_2 mixture, which according to XRD data produces mainly nanocrystalline β -W.

3.2. Influence of the deposition temperature on structural and superconducting properties of nanocrystalline β -W thin films

To analyze the influence of deposition temperature on the microstructure and the electrical transport, 160 nm thick W thin films were grown at different temperatures using an 8% N_2 mixture. Figure 3a shows the XRD for [160W8-RT], [160W8-473], [160W8-573] and [160W8-673]. All the samples display a peak that can be attributed to the $(210)_\beta$ reflection. The peak is systematically narrow and shifted to higher angles when the deposition temperature is increased. The reduction in the peak width can be related with an increment in the grain size average. The shift in the peak position and the asymmetry to higher angles can be related with crystallization α -W and overlapping of the $(210)_\beta$ and $(200)_\alpha$ reflections (see for example [160W8-673]). Figure 3b shows the temperature dependence of the normalized resistance (R/R^{10K}) for [160W8-RT], [160W8-473] and [160W8-573]. The results show that T_c decreases systematically as the deposition temperature increases. The variations could be related to the recrystallization from β -W to α -W as is evidenced from the XRD.

To understand the influence of the thermal annealing on the superconducting properties, we measure the upper critical fields (H_{c2}) in [160W8-RT] and [160W8-473]. For polycrystalline films, the anisotropy $\gamma = H_{c2}^{\parallel} / H_{c2}^{\perp}$ is related to the geometry [12]. Figure 3c shows a summary of the results. First, we will analyze $H_{c2}^{\perp}(T)$, and second, the differences between $H_{c2}^{\perp}(T)$ and $H_{c2}^{\parallel}(T)$. The temperature dependences of H_{c2}^{\perp} for dirty superconductors can be analyzed by the Werthamer-Helfand-Hohenberg (WHH) formula

$$\ln \frac{1}{t} = \sum_{v=-\infty}^{\infty} \left(\frac{1}{|2v+1|} - \left[|2v+1| + \frac{\hbar}{t} + \frac{(\alpha\hbar/t)^2}{|2v+1| + (\hbar + \lambda_{so})/t} \right]^{-1} \right) \text{ [eq. 1]}$$

where $t = T / T_c$, $\hbar = (4/\pi^2)(H_{c2}(T)/|dH_{c2}/dT|_{T_c})$, α is the Maki parameter, and λ_{so} is the spin-orbit scattering constant. When $\lambda_{so} = 0$, $H_{c2}(0)$ obtained from the WHH formula satisfies the relation $H_{c2}(0) = \frac{H_{c2}^{orb}(0)}{\sqrt{1+\alpha^2}}$ [13]. The data for both films is well described by the model using $\alpha = 0$ and $\lambda_{so} = 0$ (see dashed lines in Fig. 3c). The coherence length $\xi(0)$ values can be estimated using $\xi(0) = \sqrt{\Phi_0 / (2\pi H_{c2}^{\parallel}(0))}$ (with $\Phi_0 = 2.07 \times 10^{-7}$ G cm² is the flux quantum). The obtained values using $H_{c2}^{\perp} = 4.6$ T for [160W8-473] and 6.6 T for [160W8-RT] are 8.5 nm and 7.2 nm, respectively. We now turn to the comparison between H_{c2}^{\perp} and H_{c2}^{\parallel} . It is important to mention that both films are in the 3D limit ($\xi \ll 160$ nm). The $\gamma = H_{c2}^{\parallel} / H_{c2}^{\perp}$ is ≈ 1.7 for [160W8-RT] and ≈ 2.6 for [160W8-473]. The surface superconductivity produces a field enhancement of $H_{c3} = 1.69 H_{c2}$, which is in agreement with for [160W8-RT] [12]. On the other hand, $\gamma = 2.6$ is in agreement with the 2D limit where $H_{c2}^{\parallel}(T) \propto (1-t)^{1/2}$ [12]. The so-called vortex-free state is observed in films thinner than $\approx 4.4\xi$ (the film is too thin to nucleate a vortex core) [14], which for [160W8-473] implies the presence of superconducting paths thinner than the nominal thickness (reduction of the superconductor volume due to crystallization of α -W). We discuss the features of the 2D behavior more later when we analyze the $H_{c2}(T)$ dependences for films with different thickness.

3.3. Thickness dependence of the structural and superconducting properties of nanocrystalline β -W thin films

To understand about the influence of the dimension on the superconducting properties of nanocrystalline β -W thin films, we growth samples at room temperature using an 8% N₂ mixture with a thickness between 3 and 160 nm. The thicknesses were determined from the fits. Figure 4a shows the data for 11.8 nm and 22.8 nm thick W films. It is important to note that the best fits were obtained adding an interfacial layer of approximately 1 nm. This layer was not considered in the nominal thickness value. Figure 4b shows a summary of the thickness obtained from fits versus deposition time. The resulting growth rate average is of 21.0 (0.5) nm/min.

Figure 5 shows the XRD pattern for [11W8-RT], [23W8-RT], [70W8-RT] and [160W8-RT]. The results show reflections of the β phase. The peaks are wider as the thickness reduces. The grain sizes estimated from the (210) reflection using the equation of Scherrer are $D \approx 2$ nm for [11W8-RT] and [23W8-RT], $D \approx 8$ nm and $D \approx 9$ nm for

[70W8-RT] and [160W8-RT], respectively. The grain size average is smaller than the thickness for all the films. The fact that grain size increases with thickness could be related to the influence of the substrate and self-heating effects.

Figure 6a shows the normalized resistance of W films with different thickness. Inset Fig. 6a shows the criteria for the determination of T_c . The results show that films thicker than 17 nm show a $T_c = 4.7$ K. Below this thickness, the T_c value decreases systematically, being 3.1 K for a 3.8 nm thick W film. The superconducting transition width is $\Delta T_c = T_c - R^{zero} \approx 0.1$ K in most films. A slight broadening of the superconducting transition is observed in the thinner films, which can be attributed to enhanced thermal fluctuations when the thickness falls below the coherence length ξ [12]. The films display residual resistivity ratio ($RRR = R^{300K}/R^{10K}$) $\approx 0.93 - 1.04$, which is indicative of high disorder with very short mean free path (not shown). The resistivity of the films is independent of the thickness $\rho(300\text{ K}) \approx 150 \mu\Omega\cdot\text{cm}$.

Figures 7ab show $H_{c2}(T)$ for [8W8-RT] and [17W8-RT] with the magnetic field \mathbf{H} perpendicular (\perp) and parallel (\parallel) to the surface. The graph includes the corresponding fits using the WHH and 2D models, respectively. For the $H_{c2}^{\perp}(T)$ dependences, the $H_{c2}^{\perp}(0)$ values for [8W8-RT] and [17W8-RT] are ≈ 9 T ($\xi(0) = 6.0$ nm) and 8 T ($\xi(0) = 6.4$ nm), respectively. The comparison with [160W8-RT] (see Fig. 3c) indicates that the $H_{c2}^{\perp}(0)$ increases as the thickness decreases. This change could be attributed to the reduction in the grain size with thickness discussed above. The increment in the $H_{c2}^{\perp}(0)$ values in nanocrystalline systems reducing the grain size is also evidenced in other systems such as Mo_2N thin films [15,16].

The temperature dependence of H_{c2}^{\parallel} in the thin films with thickness lower than approximately 4.4ξ can be analyzed in the 2D limits:

$$H_{c2}^{\parallel}(T) = \frac{\sqrt{3}\Phi_0}{\pi d \left[0.855(\xi_0 l)^{\frac{1}{2}} \right]} \left(1 - T/T_c \right)^{1/2} \quad [\text{eq. 2}]$$

with $\xi(0) = (\xi_0 l)^{1/2}$ (l is the mean free path and ξ_0 the coherence length in the clean limit). The equation consider that in the dirty limit $\xi(T) = 0.855\xi(0) (1 - (T/T_c))^{-1/2}$ [12]. Although the predicted temperature dependences of superconducting parameters are for $T \rightarrow T_c$, they usually are valid over a much wider temperature range. The fits using eq. 2 for H_{c2}^{\parallel} [8W8-RT] with $\xi(0) = 6.0$ nm and [17W8-RT] with $\xi(0) = 6.4$ nm are in good agreement with the experimental data. It is important to note that for [8W8-RT], $H_{c2}^{\parallel}(2.8\text{K}) = 16$ T and the extrapolation to zero is above 26 T. These values are above

to the Pauli paramagnetic limit $H_p \approx 1.84 T_c$ (in Tesla for T_c in Kelvin) for isotropic BCS superconductors [17]. Above H_p , it is expected that the Zeeman splitting energy matches the superconducting energy gap or binding energy of a Cooper pair. The presence of very huge H_{c2} values in the vortex-free configuration suggests that the same tolerance to the magnetic field should be observed in nanocrystalline nanowires.

4. Summary

The superconducting and microstructural properties of W thin films fabricated by sputtering in N_2 :Ar mixtures were studied. The microstructure and phases are strongly affected by the gas mixture. Nanocrystalline β -W phase is obtained for N_2 concentration between 3% and 10 %. Thin films growth at RT using N_2 concentration between 20 % and 40 % display coexistence of β -W and W_2N phases. It is important to note that for N_2 concentration up to 10 %, the nitrogen stabilizes the β -W phase. This behavior is different to other metals such as tantalum [10] and molybdenum [16] where reactive mixtures of Ar/ N_2 produce nitrides.

The study of the superconducting properties is focused in nanocrystalline β -W thin films growth at RT using 8% N_2 mixtures. Coexistence of β -W and α -W phases can be induced by both thermal annealing and increment in the deposition temperature. The phase coexistence reduces the superconductor volume. The superconducting critical temperature ($T_c = 4.7$ K) is thickness independent for films thicker than ~ 17 nm. The $H_{c2}^{\perp}(T)$ dependences are well described by the WHH model for single band superconductors in the dirty limit. The extrapolated $H_{c2}(0)$ values increase as the thickness reduces, which can be related to changes in the microstructure (small grain sizes for thinner films). On the other hand, the $H_{c2}^{\parallel}(T)$ dependences, depending on thickness, are well described considering surface superconductivity and the 2D model. Our study provides a simple method for the fabrication of nanocrystalline β -W with potential applications in superconducting devices.

Acknowledgements

This work has been partially supported by Agencia Nacional de Promoción Científica y Tecnológica PICT 2015–2171 and CONICET PIP 2015-0100575CO. JAH and NH are members of the Instituto de Nanociencia y Nanotecnología CNEA-CONICET (Argentina).

Figure 1. XRD patterns for: a) Pristine [160W8-RT], [160W10-RT], [155W20-RT], [145W30-RT] and [138W50-RT]. b) Same samples annealed at 973 K. The peak deconvolution considering $\text{Cu}_{K\alpha 1}$ and $\text{Cu}_{K\alpha 2}$ for [138W50RT] is included.

Figure 2. a) Temperature dependence of the normalized resistance ($R/R^{10\text{K}}$) for W thin films growth using different N_2/Ar gas mixtures. b) Summary of T_c (right) and residual resistivity ratio ($\text{RRR} = R^{300\text{K}}/R^{10\text{K}}$) (left).

Figure 3. a) XRD patterns for W thin films growth in 8% N_2 concentration at different temperatures. b) Temperature dependence of the normalized resistance ($R/R^{10\text{K}}$). c) Temperature dependence of the upper critical field (H_{c2}) with \mathbf{H} parallel and perpendicular to the surface for [160W8-RT] and [160W8-473].

Figure 4. a) XRR patterns for W-thin films growth during 0.5 and 1 minute. b) Summary of the film thickness resulting from fits as function of the deposition time.

Figure 5. XRD patterns for [11W8-RT], [23W8-RT], [70W8-RT] and [160W8-RT]. The peak deconvolution considering $\text{Cu}_{K\alpha 1}$ and $\text{Cu}_{K\alpha 2}$ is included.

Figure 6. a) Normalized resistivity as a function of temperature for W thin films with different thickness. Inset shows the criteria used to determine the T_c . b) Summary of T_c versus thickness. Inset shows a zoom for thickness lower than 20 nm. The data for 2.8 nm is extrapolated from the temperature dependence of $R/R^{10\text{K}}$.

Figure 7. a-b) Temperature dependence of the upper critical field (H_{c2}) with \mathbf{H} parallel (\parallel) and perpendicular (\perp) to the surface for [8W8-RT] and [17W8-17], respectively. Inset a) shows typical curves of normalized resistance ($R/R^{10\text{K}}$) versus temperature for [8W8-RT] with $\mathbf{H} \parallel$ surface (from right to left $\mu_0 H = 0, 8 \text{ T}, 10 \text{ T}, 12 \text{ T}$ and 16 T).

Figure 1.

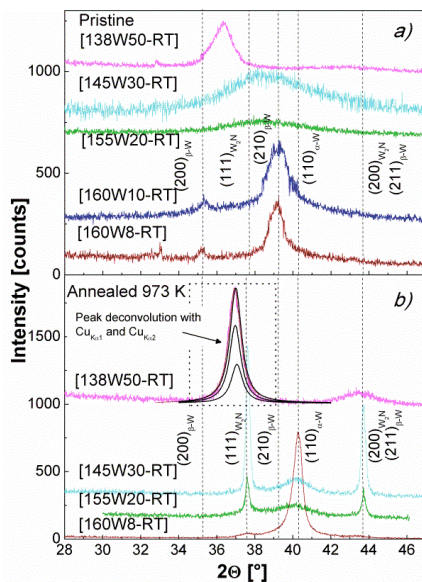


Figure 2.

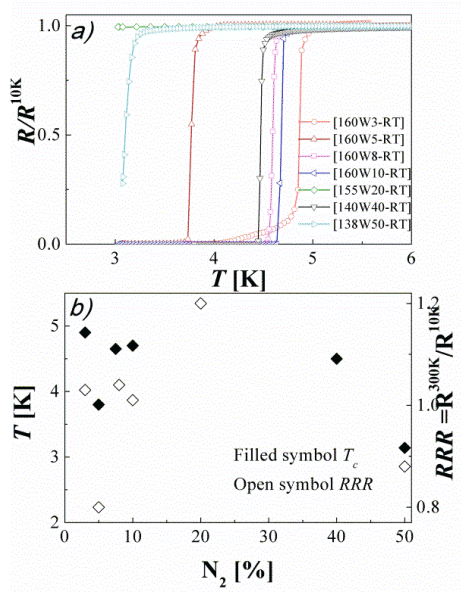


Figure 3.

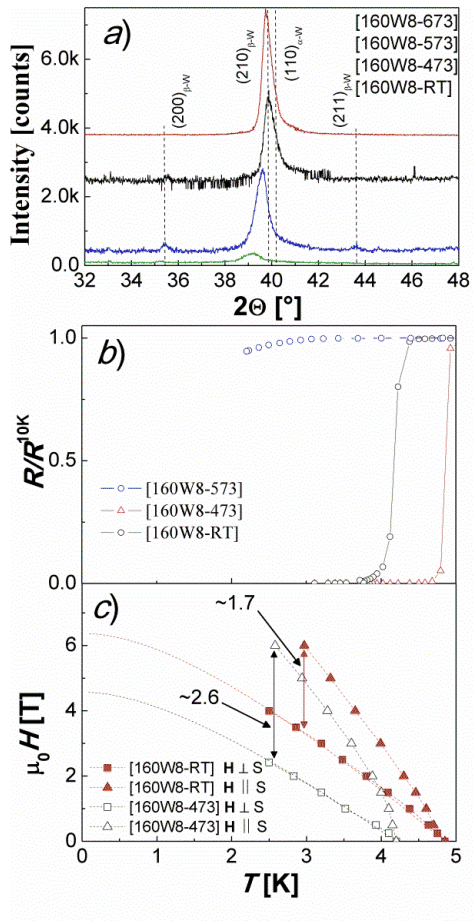


Figure 4.

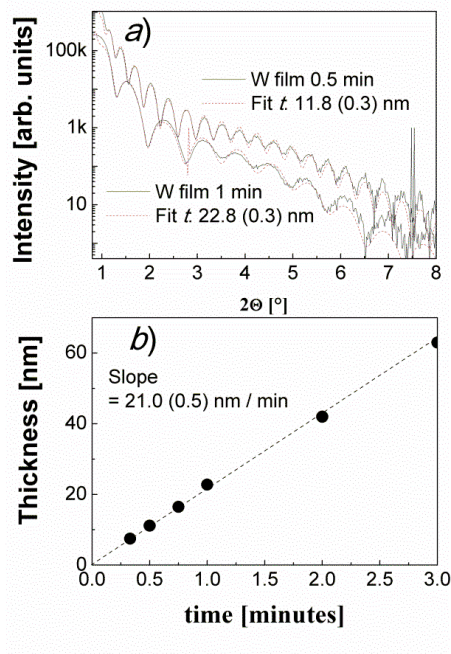


Figure 5.

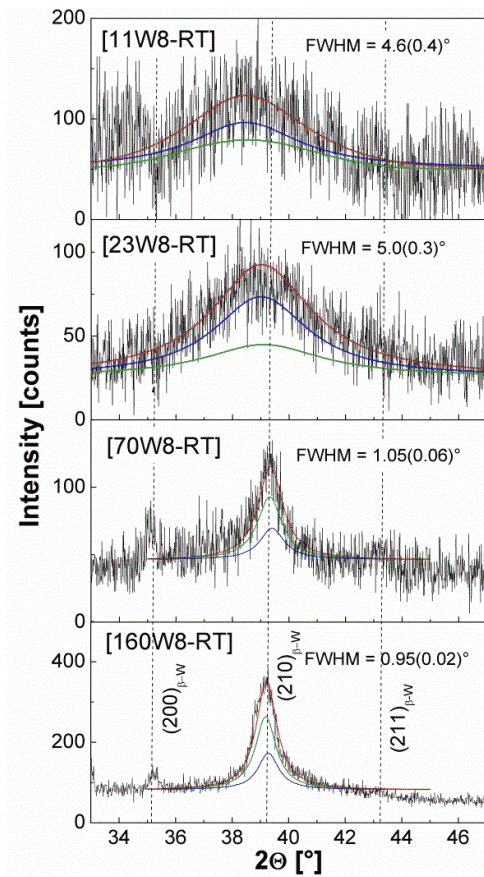


Figure 6.

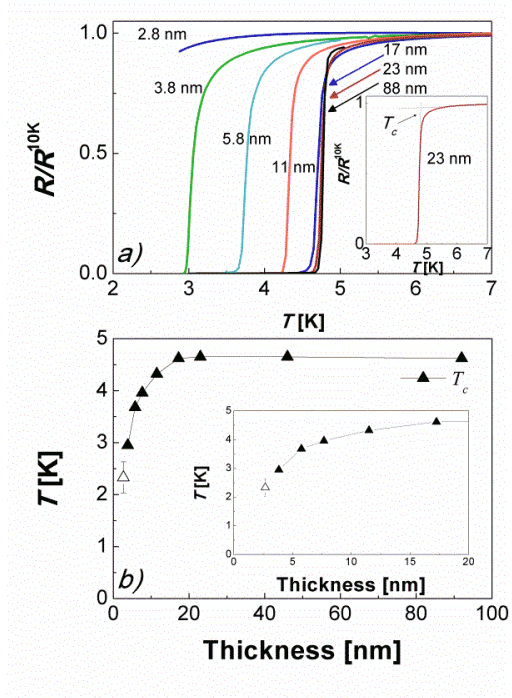
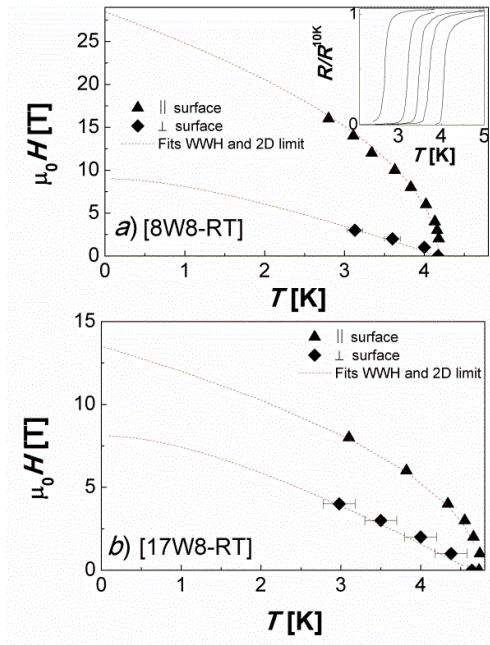


Figure 7.



-
- [1] L.C. Agudelo-Morimitsu, J. De La Roche, A. Ruden, D. Escobar, E. Restrepo-Parra, Effect of substrate temperature on the mechanical and tribological properties of W/WC produced by DC magnetron sputtering, *Ceram. Int.* **40** (2014) 7037-7042. <https://doi.org/10.1016/j.ceramint.2013.12.033>
- [2] A.L. Currie, K.E. Howard, Application of a molecular precursor to the preparation of Tungsten and beta-tungsten nitride coatings and powders, *J. Mater. Sci.* **27** (1992) 2739–2742 <https://doi.org/10.1007/BF00540699>
- [3] J. W. Gibson, R. A. Hein, Superconductivity of Tungsten, *Phys. Rev. Lett.* **12** (1964) 688-690. <https://doi.org/10.1103/PhysRevLett.12.688>
- [4] E. Sadki, S. Ooi, K. Hirata, Focused-ion-beam-induced deposition of superconducting nanowires, *Appl. Phys. Lett.* **85** (2004) 6206-6208. <https://doi.org/10.1063/1.1842367>
- [5] Shamashis Sengupta, Chuan Li, Cedric Baumier, Alik Kasumov, S. Gueron, H. Bouchiat, F. Fortuna, Superconducting nanowires by electron-beam-induced deposition, *Appl. Phys. Lett.* **106** (2015) 042601. <https://doi.org/10.1063/1.4906269>
- [6] Yi Sun, Jian Wang, Weiwei Zhao, Mingliang Tian, Meenakshi Singh, Moses H. W. Chan, Voltage-current properties of superconducting amorphous tungsten nanostrips, *Sci Rep* **3** (2013) 2307. DOI: 10.1038/srep02307
- [7] K. Salamon, O. Milat, N. Radic, P. Dubcek, M. Jercinovic, S. Bernstorff, Structure and morphology of magnetron sputtered W films studied by x-ray methods, *J. Phys. D: Appl. Phys.* **46** (2013) 095304 (10pp). <https://doi.org/10.1088/0022-3727/46/9/095304>
- [8] Yong Jin Kim, Sung-Gyu Kang, Yeonju Oh, Gyu Won Kim, In Ho Cha, Heung Nam Han, Young Keun Kim, Microstructural evolution and electrical resistivity of nanocrystalline W thin films grown by sputtering, *Mater. Charact.* **145** (2018) 473–478. <https://doi.org/10.1016/j.matchar.2018.09.016>
- [9] N. Radic, A. Tonejc, J. Ivkov, P. Dubcek, S. Bernstorff, Z. Medunic, Sputter-deposited amorphous-like tungsten, *Surf. Coat. Tech* **180-181** (2004) 66–70. <https://doi.org/10.1016/j.surfcoat.2003.10.038>
- [10] F.M. Kilbane, P. S. Habig, Superconducting transition temperatures of reactively sputtered films of tantalum nitride and tungsten nitride, *J. Vac Scie Tech* **12** (1974) 107-109. <https://doi.org/10.1116/1.568734>
- [11] C. Braun, Parratt32 for the Reflectometry Tool, HMI, Berlin, 1997-1999, <http://www.helmholtz-berlin.de>.
- [12] M. Tinkham 2004 Introduction to superconductivity, 2 edition ed. (Dover Publications, New York).

-
- [13] K. Maki, Effect of Pauli Paramagnetism on Magnetic Properties of High-Field Superconductors, *Phys. Rev.* **148** (1966) 362-369. <https://doi.org/10.1103/PhysRev.148.362>
- [14] N. Takezawa, T. Koyama, M. Tachiki. Angular dependence of the upper critical field in layered superconductors. *Physica C* **207** (1993) 231-238. [https://doi.org/10.1016/0921-4534\(93\)90304-9](https://doi.org/10.1016/0921-4534(93)90304-9)
- [15] R. Baskaran, A.V. Thanikai Arasu, E.P. Amaladass, L.S. Vaidhyanathan, D.K. Baisnab, Increased upper critical field for nanocrystalline MoN thin films deposited on AlN buffered substrates at ambient temperature, *J. Phys. D* **49** (2016) 205304–205307. <https://doi.org/10.1088/0022-3727/49/20/205304>
- [16] N. Haberkorn, S. Bengio, H. Troiani, S. Suárez, P.D. Pérez, P. Granell, F. Golmar, M. Sirena, J. Guimpel, Thickness dependence of the superconducting properties of γ -Mo₂N thin films on Si (001) grown by DC sputtering at room temperature, *Mater. Chem. Phys.* **204** (2018) 48–57. <https://doi.org/10.1016/j.matchemphys.2017.10.015>
- [17] A.M. Clogston, Upper limit for critical field in hard superconductors, *Phys. Rev. Lett.* **9** (1962) 266-267. <https://doi.org/10.1103/PhysRevLett.9.266>